Multiband effects and the Bose-Hubbard model in one-dimensional lattices

Wei Xu, Maxim Olshanii, and Marcos Rigol

Phys. Rev. A **94**, 031601 — Published 2 September 2016

DOI: 10.1103/PhysRevA.94.031601

Multiband Effects and the Bose-Hubbard Model in One-Dimensional Lattices

Wei Xu,[1] Maxim Olshanii,[2] and Marcos Rigol[1]

[1] *Department of Physics, The Pennsylvania State University, University Park, PA 16802, USA*
[2] *Department of Physics, University of Massachusetts, Boston, MA 02125, USA*

We study phase diagrams of one-dimensional bosons with contact interactions in the presence of a lattice. We use the Worm algorithm in continuous space and focus on the incommensurate superfluid-Mott-insulator transition. Our results are compared to those from the one-band Bose-Hubbard model. When Wannier states are used to determine the Bose-Hubbard model parameters, the comparison unveils an apparent breakdown of the one-band description for strong interactions, even for the Mott insulating state with an average of one particle per site ($n = 1$) in deep lattices. We introduce an inverse confined scattering analysis to obtain the ratio U/J, with which the Bose-Hubbard model provides correct results for strong interactions, deep lattices, and $n = 1$.

a. Introduction. Simplified one-band (or few-bands) effective lattice models such as the Fermi-Hubbard and t-J models for strongly interacting fermions [1, 2] and the Bose-Hubbard model for strongly interacting bosons [3, 4] have played a central role in our understanding of the interplay between quantum fluctuations, interactions, and lattice effects in a wide range of physical systems ranging from solid state materials to optical lattices. Unfortunately, many-body interactions make it difficult to establish the limits of applicability of such models, as well as to explore how changes in the way effective parameters are calculated extend their relevance. With those questions in mind, here we study 1D systems of bosons with contact interactions in the presence of a lattice.

Effective 1D Bose systems with contact interactions are created in experiments with ultracold gases in deep two-dimensional optical lattices [4–6]. An additional (weaker) optical lattice has been used to drive superfluid-Mott-insulator transitions [7–9]. Such transitions are best understood for weak contact interactions and deep lattices, a regime that can be modeled using the one-band Bose-Hubbard model [10, 11]. The phase diagram of this model has been studied in great detail using a wide variety of computational techniques [12–16]. It is well established that the phase transition driven by changing the site occupancies (incommensurate transition) belongs to the mean-field universality class, while the one with constant integer filling (commensurate transition) belongs to $(d+1)XY$ universality class [4].

Beyond the one-band approximation, it is known that in 1D an arbitrarily weak lattice can lead to the formation of a Mott-insulating phase in the strong interaction regime at integer fillings [8, 17]. This "pinning" transition is described by the (1+1) quantum sine-Gordon model [4, 18], and has been studied very recently [9, 19]. Multiband effects have also been seen in collapse and revival experiments in three dimensions, in which they were recast into renormalized multi-body interactions [20, 21], and in theoretical studies of quench dynamics [22–24]. Together with other effects such as density-induced tunneling, as well as long-range interactions and tunneling [25], these studies have highlighted the necessity to go beyond the standard Bose-Hubbard model to describe many experiments (for a recent review, see Ref. [26]).

In this letter, we focus on the incommensurate Mott insulator transition in continuous space. To study it, we use path integral quantum Monte Carlo simulations (QMC) with worm updates [27–29], as detailed in Ref. [30]. We compute phase diagrams obtained by changing the lattice depth while keeping the contact interaction strength constant. We consider systems with fillings of up to two bosons per site. We show that for strong contact interactions, even for deep lattices and an average of one particle per site ($n = 1$), there are significant deviations from the Bose-Hubbard model predictions for the phase diagram when the parameters of that model are determined using Wannier functions. We introduce an inverse confined scattering analysis that allows one to restore the validity of the Bose-Hubbard model for strong interactions, deep lattices, and $n = 1$.

b. Model Hamiltonian. We consider bosons with repulsive contact interactions in the presence of an external periodic potential $V_{\rm ext}(x) = V_0 \sin^2(kx)$:

$$H = \sum_{i=1}^{N} \left[-\frac{\hbar^2}{2m}\frac{\partial^2}{\partial x_i^2} + V_{\rm ext}(x_i) \right] + g \sum_{i<j=1}^{N} \delta(x_i - x_j)\,, \quad (1)$$

where N is the number of particles, V_0 is the lattice depth, and $k = 2\pi/\lambda$, with λ being the lattice wavelength (the lattice spacing is then $a = \lambda/2$). In the absence of $V_{\rm ext}(x)$, H reduces to the Lieb-Liniger model, which is integrable via Bethe ansatz [31]. g is the strength of the contact interactions, which is related to the effective 1D scattering length $a_{\rm 1D}$ via $g = -2\hbar^2/ma_{\rm 1D}$, and to the Lieb-Liniger parameter γ via $\gamma = mg/(\hbar^2\rho)$ [4]. In the weak interaction and deep lattice limit, H can be mapped onto the one-band Bose-Hubbard Hamiltonian

$$H_{\rm BH} = -J \sum_i \left(a_i^\dagger a_{i+1} + {\rm H.c.} \right) + \frac{U}{2} \sum_i n_i \left(n_i - 1 \right), \quad (2)$$

where J is the nearest neighbor tunneling amplitude and U the the strength of the on-site repulsive interaction [11]. In the shallow lattice limit, as mentioned before, H reduces to (1+1) sine-Gordon Hamiltonian [8, 18]. This model predicts that the pinning transi-

tion occurs for $\gamma > \gamma_c \approx 3.5$ [17]. Away from those limits, exact results for phase diagrams can be obtained using QMC in continuous space [27–29]. In cubic lattices, related phase diagrams have been reported in Refs. [32, 33].

c. Indicators. We have used two indicators to locate the transition between the superfluid and insulating phases. (i) The zero-momentum Matsubara Green's function. It requires the calculation of the momentum space Green's function $G(p,\tau)$ [34]. Since the ground-state has zero total momentum, here we focus on $G(p=0,\tau)$. In the vicinity of the transition point, within the Mott insulating phase, $G(p=0,\tau)$ decays exponentially with the imaginary time τ as $\tau \to \pm\infty$: $G(p=0,\tau) \to Z_{\pm}\exp(\mp\epsilon_{\pm}\tau)$, where $\epsilon_{\pm}$ is the single-particle/hole excitation energy. In the grand canonical ensemble, $\epsilon_{\pm}$ is defined relative to the chemical potential μ with $\epsilon_{\pm} = |\mu - \mu_{\pm}|$, where $\mu_{\pm}$ gives the upper/lower boundary of the Mott lobe. To prove the robustness of the method, we chose different chemical potentials μ and obtained essentially the same phase boundary $\mu_{\pm}$ [35]. We also simulated different system sizes with $L/a = 24, 30, 42, 60$ lattice sites, finding that for $L/a \gtrsim 42$ finite-size effects are negligible [35]. All results reported from this approach are obtained from systems with $L/a = 60$. (ii) The superfluid density $\rho_s = mL\langle W^2\rangle/(\hbar^2\beta)$ [27], where $\langle W^2\rangle$ is the winding number estimator and L is the system size. In the thermodynamic limit, ρ_s is nonzero in the superfluid phase and vanishes in the Mott insulating phase. In finite systems, ρ_s satisfies a scaling relation in the critical regime [36]: $\rho_s L^{\xi/\nu} = F(|\mu - \mu_c|L^{1/\nu})$, where the critical exponent $\xi = \nu(d+z-2)$, $d=1$ is the dimension, and the correlation length and dynamical critical exponents are $\nu = 1/2$ and $z = 2$, respectively, for the incommensurate transition. At the critical point, $\rho_s L^{\xi/\nu}$ is independent of the system size. Thus, one can obtain the transition point from the crossing of curves for different system sizes [35].

To determine critical points, it is less computationally demanding to use $G(p=0,\tau)$ than the finite-size scaling analysis of ρ_s. In the former approach one only needs to do a calculation for a sufficiently large system size for one value of μ close to the phase boundary to determine μ_+ or μ_-, while in the latter multiple simulations with different values of μ and L are needed to locate the crossing point. We then use $G(p=0,\tau)$ for constructing the phase diagrams, while the scaling of ρ_s is mainly used to check results of the former approach.

d. Phase diagrams. As mentioned before, we are interested in the phase diagrams obtained by changing the lattice depth while keeping a_{1D} (and, hence, γ) constant, as done in most optical lattice experiments [3, 4]. In Fig. 1, we report the phase diagrams obtained for three values of a_{1D}, and for Mott insulating states with one particle ($n=1$, main panel) and two particles ($n=2$, inset) per lattice site. Note that, contrary to the usual way in which phase diagrams are reported, in Fig. 1 we plot the phase boundaries in terms of $\mu - \mu_0^c$, where μ_0^c is the critical chemical potential for the vacuum boundary

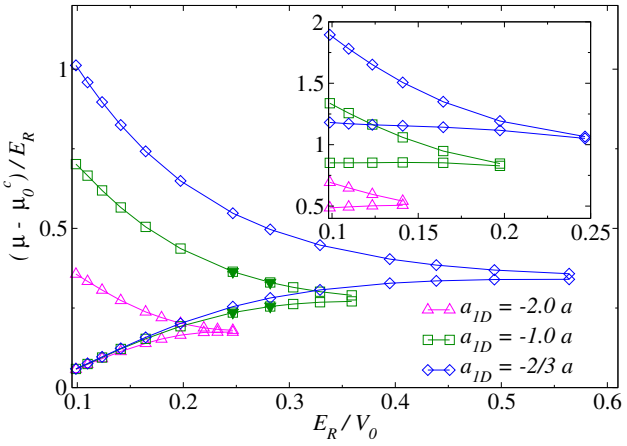

FIG. 1. (Color online) Mott lobes for one particle ($n=1$, main panel) and two particles ($n=2$, inset) per site. The lobes are obtained at fixed effective 1D scattering length $a_{1D}/a = -2.0,\ -1.0,\ -2/3$ (for $n=1$, $\gamma = 1, 2$, and 3, respectively). The points are obtained from the zero-momentum Green function (open symbols) and the scaling of the superfluid density (filled symbols). $E_R = \hbar^2k^2/(2m)$ is the recoil energy and μ_0^c is the chemical potential at the vacuum boundary for each value of V_0 (determined from the zero-momentum Green function). Lines between symbols are to guide the eye.

as obtained in our simulations (it is independent of a_{1D}). This allows us to reduce a small chemical potential bias introduced by the finite discretization $\Delta\tau$ of imaginary time in our QMC approach. Such a bias vanishes linearly with $\Delta\tau$ and, for the small but finite values of $\Delta\tau$ used in our simulations, it is negligible when chemical potential differences are reported [35]. In Fig. 1, open symbols depict points obtained using $G(p=0,\tau)$, while the four filled symbols for $a_{1D} = -a$ depict points obtained with the scaling of ρ_s. The latter can be seen to lead to results indistinguishable to those from $G(p=0,\tau)$. Figure 1 shows that, as expected, the Mott lobes grow with increasing γ. Also, the lower boundary of the $n=1$ Mott lobe becomes independent of γ for deep lattices. All Mott lobes studied here have a finite extent because $\gamma < \gamma_c$.

e. Gap and the one-band Bose-Hubbard model. Having determined the phase diagrams, we compare the predictions of the QMC simulations with those from the one-band Bose-Hubbard model. In order to minimize the number of parameters that need to be computed for the comparison, we focus on the Mott gap: $E_g = \mu_+ - \mu_-$. As a first estimation, U and J are calculated within the one-band approximation using maximally localized Wannier states [37, 38]. The Bose-Hubbard phase diagram [15] is then translated into the parameters in the continuum. The results for $n=1$ and $n=2$ are presented in the main panels of Fig. 2(a) and 2(b), respectively, and are compared to the QMC results derived from Fig. 1.

For $a_{1D}/a = -2.0$ and $n=1$ ($\gamma = 1$), the gap predicted by both approaches is nearly indistinguishable for all lattice depths. The same is expected to be true for even smaller values of a_{1D}, so we focus on higher fillings

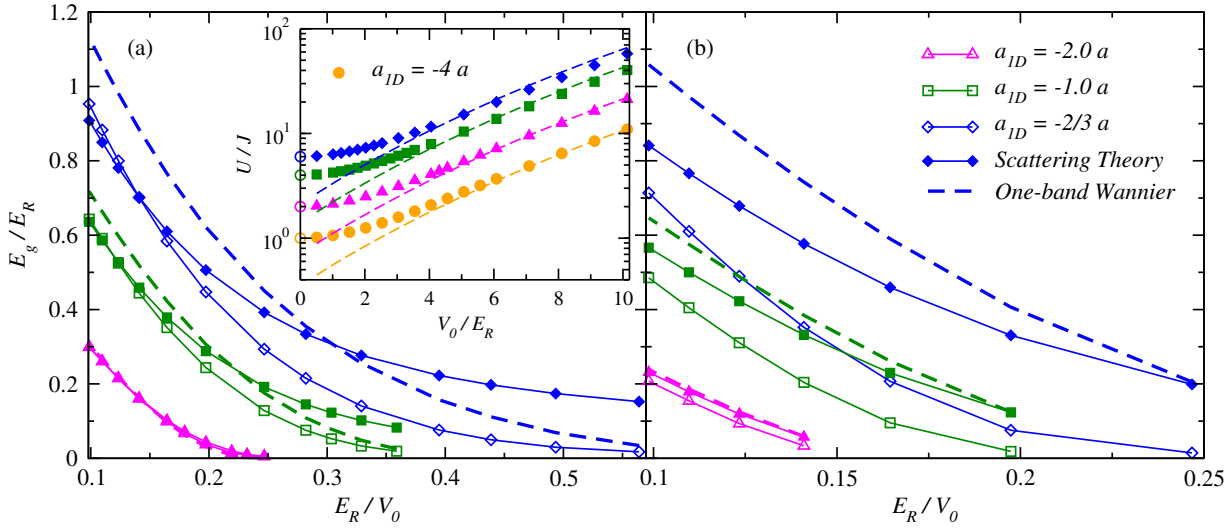

FIG. 2. (Color online) Mott gaps at fillings $n = 1$ (a) and $n = 2$ (b) vs E_R/V_0 for $a_{1D}/a = -2.0,\ -1.0,\ -2/3$. The open symbols depict the results from QMC simulations. The dashed lines depict the Hubbard model prediction [15] translated into the continuum using U and J as obtained from maximally localized Wannier functions [37, 38]. Filled symbols depict the Hubbard model prediction [15] translated into the continuum using U/J from the two-particle scattering analysis explained in the text, and U obtained from the exact solution of two interacting bosons in a harmonic trap. Inset in (a): comparison between U/J as obtained from the Wannier functions (dashed lines) and from the two-particle scattering analysis (filled symbols, consistent with those in the main panel). Open circles for $V_0/E_R = 0$ show the no-lattice asymptotic limit from scattering theory.

and higher values of a_{1D}. For $n = 2$ and $a_{1D}/a = -2.0$ ($\gamma = 1/2$), already a small deviation can be seen between the gap obtained from QMC and the Hubbard model prediction. Striking differences, on the other hand, can be seen for $\gamma = 2$ and 3, particularly for the deepest lattices and $n = 2$. Counter-intuitively, in Fig. 2(a), the gap predicted by the Hubbard model becomes increasingly larger than the exact one as the lattice depth is increased (the one-band prediction worsens as the lattice depth is increased). This suggests that, with increasing V_0, the one-band approximation leads to an increasing overestimation of U/J, and, hence, of the gap (we will come back to this point later). Hence, our results show that, for $\gamma \gtrsim 1$, the closest agreement between the exact solution and the Hubbard model prediction is obtained for the weakest lattices, for which the one-band approximation is most uncontrolled.

f. Inverse confined scattering analysis. When using Wannier functions, the fact that one neglects the effect of interactions is what leads to the overestimation of U/J inferred from Fig. 2. In order to account for interactions in the calculation of U/J, so that the values of U/J are the appropriate ones in the limit of deep lattices, we use an inverse scattering approach. The idea is to obtain U/J by comparing the exact low-energy scattering amplitude from the Bose-Hubbard model ($a_{\rm BH}$) and that of the continuum model ($a_{\rm CM}$) in Eq. (1). Our approach is different from the one followed in Refs. [39, 40], where scattering analyses were carried out for Feshbach resonances.

As in Refs. [41, 42], we define the 1D analog of the three-dimensional scattering length a_{3D}. For a translational invariant system, the scattering wavefunction for two bosons with total momentum zero can be written as (in the principal domain $x_1 > x_2$)

$$\psi^{(2)}(x_1, x_2) = e^{i\theta(q)}\phi_q(x_1)\phi_{-q}(x_2) + \text{c.c.}\,, \qquad (3)$$

where $\phi_q(x)$ is the plane-wave eigenfunction with positive momentum q and energy $\epsilon(q)$. For any non-vanishing interaction, the scattering phase $\theta(q)$ is finite and goes asymptotically to zero as momentum q approaches zero. The scattering length a_{1D} characterizes the first nontrivial term in the Taylor expansion of the scattering phase in powers of the momentum q,

$$a_{1D} = -\lim_{q\to 0^+} \theta(q)/q\,. \qquad (4)$$

This definition gives the effective scattering length a_{1D} of the Lieb-Liniger model, which was introduced previously. Discretizing the Lieb-Liniger Hamiltonian one obtains the Bose-Hubbard model and its corresponding scattering length $a_{\rm BH} = -4Ja/U$ [43].

When an external lattice is added, the propagating part of the two-body wavefunction has the same form as Eq. (3), but with $\phi_q(x)$ being a Bloch-state eigenfunction and $\epsilon(q)$ being its corresponding eigenenergy. For q different from half-integer multiples of the lattice wavevector k, $\phi_q(x)$ and $\phi_{-q}(x)$ can be shown to be linearly independent. In addition to the propagating part, there is also a localized part of the two-body wavefunction. It has a total energy $2\epsilon(q)$ but complex one-body energies $\zeta(\eta)$ and $\zeta(-\eta) \equiv \zeta(\eta)^\star$, where $\zeta(\eta) = \epsilon(q) + i\eta$ with $\eta > 0$. For each $\zeta(\eta)$, one can find two linearly inde-

pendent Bloch eigenstates of the one-body Hamiltonian, $H_0 = -\hbar^2/(2m)(\partial^2/\partial x^2) + V_{\rm ext}(x)$, labeled as $\chi[k(\eta), x]$ and $\chi[-k(\eta), x] \equiv \chi[k(\eta), -x]$. They are related by a mirror reflection, where $k(\eta)$ is a Bloch momentum and $\chi[k(\eta), x]$ is a Bloch state corresponding to it. The (boson) symmetric localized part of the two-body wavefunction has the form (in the principal domain $x_1 > x_2$)

$$\chi^{(2)}(x_1, x_2, \eta) = \chi[k(\eta), x_1]\chi[k(-\eta), x_2] + \text{c.c.}\,. \quad (5)$$

In general, there are two possible choices of the Bloch momentum $k(\eta)$ for each energy. For simplicity, we require that the imaginary part $\text{Im}[k(\eta)] > 0$ for $\eta > 0$ [44]. We assume that the Bloch vector of the center-of-mass motion vanishes, and, as a result, the two-body scattering state is a periodic function of the center-of-mass coordinate. This leads, in turn, to the requirement that the real part of the corresponding Bloch momentum be a half-integer of k, i.e., $\text{Re}[k(\eta_l)] = lk/2$ for $l > 0$. The full two-body scattering state can then be written as a combination of the propagating and localized components,

$$\Psi^{(2)}(x_1, x_2) = \psi^{(2)}(x_1, x_2) + \sum_{l=1}^{\infty} A_l\, \chi^{(2)}(x_1, x_2, \eta_l)\,. \quad (6)$$

$\Psi^{(2)}(x_1, x_2)$ is an eigenstate of the two-body Hamiltonian with a real eigenvalue outside of the interaction line $x_1 = x_2$. Next, we introduce the relative $r = x_1 - x_2$ and center-of-mass $R = (x_1 + x_2)/2$ coordinates, and define $\psi_+(R, r) \equiv \phi_q(R + \frac{r}{2})\phi_{-q}(R - \frac{r}{2})$, of which we need $\psi_+(R) \equiv \lim_{q\to 0^+} \psi_+(R, r)\big|_{r=0}$, and $\psi'_+(R) \equiv \lim_{q\to 0^+} \partial_r \psi_+(R, r)\big|_{r=0}$. The jump boundary condition [35] imposes the following relationship between $a_{\rm CM}$ and the coefficients A_l of the expansion (6),

$$\begin{aligned}\psi_+(R) a_{\rm CM} = &\lim_{q\to 0^+} \frac{\psi'_+(R)}{iq} a_{1\rm D} \\ &- \sum_{l=1}^{\infty} \left[\chi_l^{(2)}(R) + a_{1\rm D}\chi_l'^{(2)}(R)\right] \tilde{A}_l\,,\end{aligned} \quad (7)$$

where $\chi_l^{(2)}(R) = \lim_{q\to 0^+} \chi^{(2)}(R + \frac{r}{2}, R - \frac{r}{2}, \eta_l)\big|_{r=0}$, $\chi_l'^{(2)}(R) = \lim_{q\to 0^+} \partial_r \chi^{(2)}(R + \frac{r}{2}, R - \frac{r}{2}, \eta_l)\big|_{r=0}$, and $\tilde{A}_l = \lim_{q\to 0^+} iA_l/(2q)$. Since all functions of R in Eq. (7) have at least a periodicity of π/k (and are even), a way to solve that equation numerically is using Fourier expansions. For a given number $l_{\rm max}$ of terms in the sum in Eq. (6), one needs to keep the same number of terms in the Fourier expansion of all the functions. As a result, one obtains an inhomogeneous $(l_{\rm max}+1)\times(l_{\rm max}+1)$ system of linear algebraic equations, the solution of which gives $a_{\rm CM}(l_{\rm max})$. We then extrapolate the results to $l_{\rm max} \to \infty$ to obtain $a_{\rm CM}$ (see Ref. [35] for more details).

In the inset in Fig. 2(a), we compare U/J as obtained from the scattering and Wannier analyses for the same values of $a_{1\rm D}/a$ as in the main panels, as well as for $a_{1\rm D}/a = -4$. For weak interactions ($a_{1\rm D}/a \lesssim -2$) and deep enough lattices ($V_0/E_R \gtrsim 5$), one can see that the results from both approaches are nearly indistinguishable. On the other hand, for $a_{1\rm D}/a > -2$ one can see that the Wannier analysis increasingly overestimates U/J as the lattice depth and $a_{1\rm D}$ are increased. This can be intuitively understood because interactions make the wavefunction of two particles in a site increasingly rigid to deformation as the lattice depth is increased. In that strongly interacting regime, the Wannier function calculations are not reliable even for deep lattices. As expected, independently of the value of $a_{1\rm D}$, U/J from the inverse scattering analysis strongly deviates from the Wannier predictions for weak lattices. In the limit of vanishing lattice depth, the former predicts $U/J = -4a/a_{1\rm D}$.

In the main panels of Fig. 2, we show the Bose-Hubbard model predictions for the phase diagram translated into the continuum using the scattering analysis results for U/J, and U obtained using the ground-state wavefunction of two interacting bosons in a harmonic trap [35, 45]. For $n = 1$ [Fig. 2(a)] and $\gamma = 1$, there is almost no visible difference with the Wannier results. On the other hand, for $\gamma = 2$ and deep enough lattices, the Hubbard model with the improved values of U/J and U correctly predicts the value of the gap. For the deepest lattices for $\gamma = 3$, we find a small deviation between the gap predicted by QMC and by the Bose-Hubbard model. Its most likely origin is the failure of the harmonic potential to correctly predict U. Further studies are needed to find more accurate ways to determine U. For $n = 2$ and $a_{1\rm D}/a \gtrsim -2$, the Bose-Hubbard results are clearly inadequate independently of how U/J and U are calculated.

In conclusion, our *ab initio* calculation of the phase diagram of 1D bosons in an optical lattice shows that, for $n \lesssim 1$, the one-band Bose-Hubbard model remains useful as an effective theory far into the multiband regime – provided that its parameters are properly renormalized to account for the contributions of the excited bands. Here, the renormalized parameters are obtained from an inverse confined scattering analysis. For $n \gtrsim 2$ and $\gamma > 1/2$, our results highlight the need for a more refined effective theory than the traditional one-band Hubbard model. Having found experimentally relevant regimes [9, 46] in which the traditional Bose-Hubbard model fails, our study is a first step in the needed exploration of beyond Bose-Hubbard model physics in 1D lattices in the presence of strong interactions and/or high fillings.

ACKNOWLEDGMENTS

This work was supported by the U.S. Office of Naval Research. The computations were performed in the Institute for CyberScience at Penn State. We thank Nikolay Prokof'ev for providing the worm algorithm code used in the calculations, Satoshi Ejima for sharing with us the critical values of U/J reported in Ref. [15], and Juan Carrasquilla, Vanja Dunjko, Zhiyuan Yao and Chao Zhang for discussions.

[1] E. Dagotto, "Correlated electrons in high-temperature superconductors," Rev. Mod. Phys. **66**, 763–840 (1994).

[2] M. Imada, A. Fujimori, and Y. Tokura, "Metal-insulator transitions," Rev. Mod. Phys. **70**, 1039–1263 (1998).

[3] I. Bloch, J. Dalibard, and W. Zwerger, "Many-body physics with ultracold gases," Rev. Mod. Phys. **80**, 885–964 (2008).

[4] M. A. Cazalilla, R. Citro, T. Giamarchi, E. Orignac, and M. Rigol, "One dimensional bosons: From condensed matter systems to ultracold gases," Rev. Mod. Phys. **83**, 1405–1466 (2011).

[5] H. Moritz, T. Stöferle, M. Köhl, and T. Esslinger, "Exciting collective oscillations in a trapped 1d gas," Phys. Rev. Lett. **91**, 250402 (2003).

[6] T. Kinoshita, T. Wenger, and D. S. Weiss, "Observation of a one-dimensional Tonks-Girardeau gas," Science **305**, 11251128 (2004).

[7] T. Stöferle, H. Moritz, C. Schori, M. Köhl, and T. Esslinger, "Transition from a strongly interacting 1D superfluid to a Mott insulator," Phys. Rev. Lett. **92**, 130403 (2004).

[8] E. Haller, R. Hart, M. J. Mark, J. G. Danzl, L. Reichsöllner, M. Gustavsson, M. Dalmonte, G. Pupillo, and H.-C. Nägerl, "Pinning quantum phase transition for a Luttinger liquid of strongly interacting bosons," Nature **466**, 597–600 (2010).

[9] G. Boéris, L. Gori, M. D. Hoogerland, A. Kumar, E. Lucioni, L. Tanzi, M. Inguscio, T. Giamarchi, C. D'Errico, G. Carleo, G. Modugno, and L. Sanchez-Palencia, "Mott transition for strongly interacting one-dimensional bosons in a shallow periodic potential," Phys. Rev. A **93**, 011601 (2016).

[10] M. P. A. Fisher, P. B. Weichman, G. Grinstein, and D. S. Fisher, "Boson localization and the superfluid-insulator transition," Phys. Rev. B **40**, 546–570 (1989).

[11] D. Jaksch, C. Bruder, J. I. Cirac, C. W. Gardiner, and P. Zoller, "Cold bosonic atoms in optical lattices," Phys. Rev. Lett. **81**, 3108 (1998).

[12] G. G. Batrouni, R. T. Scalettar, and G. T. Zimanyi, "Quantum critical phenomena in one-dimensional Bose systems," Phys. Rev. Lett. **65**, 1765–1768 (1990).

[13] N. Elstner and H. Monien, "Dynamics and thermodynamics of the Bose-Hubbard model," Phys. Rev. B **59**, 12184–12187 (1999).

[14] T. D. Kühner, S. R. White, and H. Monien, "One-dimensional Bose-Hubbard model with nearest-neighbor interaction," Phys. Rev. B **61**, 12474 (2000).

[15] S. Ejima, H. Fehske, and F. Gebhard, "Dynamic properties of the one-dimensional Bose-Hubbard model," EPL (Europhysics Letters) **93**, 30002 (2011).

[16] J. Carrasquilla, S. R. Manmana, and M. Rigol, "Scaling of the gap, fidelity susceptibility, and bloch oscillations across the superfluid-to-Mott-insulator transition in the one-dimensional Bose-Hubbard model," Phys. Rev. A **87**, 043606 (2013).

[17] H. P. Büchler, G. Blatter, and W. Zwerger, "Commensurate-incommensurate transition of cold atoms in an optical lattice," Phys. Rev. Lett. **90**, 130401 (2003).

[18] T. Giamarchi, *Quantum Physics in One Dimension* (Oxford University Press (OUP), 2003).

[19] G. E. Astrakharchik, K. V. Krutitsky, M. Lewenstein, and F. Mazzanti, "One-dimensional Bose gas in optical lattices of arbitrary strength," Phys. Rev. A **93**, 021605 (2016).

[20] S. Will, T. Best, U. Schneider, L. Hackermüller, D. Lühmann, and I. Bloch, "Time-resolved observation of coherent multi-body interactions in quantum phase revivals," Nature **465**, 197–201 (2010).

[21] P. R. Johnson, D. Blume, X. Y. Yin, W. F. Flynn, and E. Tiesinga, "Effective renormalized multi-body interactions of harmonically confined ultracold neutral bosons," New J. Phys. **14**, 053037 (2012).

[22] M. Łacki and J. Zakrzewski, "Fast dynamics for atoms in optical lattices," Phys. Rev. Lett. **110**, 065301 (2013).

[23] M. Łacki, D. Delande, and J. Zakrzewski, "Dynamics of cold bosons in optical lattices: effects of higher Bloch bands," New J. Phys. **15**, 013062 (2013).

[24] J. Major, M. Łacki, and J. Zakrzewski, "Reexamination of the variational Bose-Hubbard model," Phys. Rev. A **89**, 043626 (2014).

[25] T. Sowiński, "Quantum phase transition in a shallow one-dimensional optical lattice," J. Opt. Soc. Am. B **32**, 670 (2015).

[26] O. Dutta, M. Gajda, P. Hauke, M. Lewenstein, D.-S. Lühmann, B. A. Malomed, T. Sowiński, and J. Zakrzewski, "Non-standard Hubbard models in optical lattices: a review," Rep. Prog. Phys. **78**, 066001 (2015).

[27] D. M. Ceperley, "Path integrals in the theory of condensed helium," Rev. Mod. Phys. **67**, 279–355 (1995).

[28] M. Boninsegni, N. Prokof'ev, and B. Svistunov, "Worm algorithm for continuous-space path integral Monte Carlo simulations," Phys. Rev. Lett. **96**, 070601 (2006).

[29] M. Boninsegni, N. V. Prokof'ev, and B. V. Svistunov, "Worm algorithm and diagrammatic Monte Carlo: A new approach to continuous-space path integral Monte Carlo simulations," Phys. Rev. E **74**, 036701 (2006).

[30] W. Xu and M. Rigol, "Universal scaling of density and momentum distributions in Lieb-Liniger gases," Phys. Rev. A **92**, 063623 (2015).

[31] E. H. Lieb and W. Liniger, "Exact analysis of an interacting Bose gas. I. The general solution and the ground state," Phys. Rev. **130**, 1605 (1963).

[32] S. Pilati and M. Troyer, "Bosonic superfluid-insulator transition in continuous space," Phys. Rev. Lett. **108**, 155301 (2012).

[33] T. T. Nguyen, A. J. Herrmann, M. Troyer, and S. Pilati, "Critical temperature of interacting Bose gases in periodic potentials," Phys. Rev. Lett. **112**, 170402 (2014).

[34] B. Capogrosso-Sansone, N. V. Prokof'ev, and B. V. Svistunov, "Phase diagram and thermodynamics of the three-dimensional Bose-Hubbard model," Phys. Rev. B **75**, 134302 (2007).

[35] See supplemental material.

[36] I. Hen, M. Iskin, and M. Rigol, "Phase diagram of the hard-core Bose-Hubbard model on a checkerboard superlattice," Phys. Rev. B **81**, 064503 (2010).

[37] R. Walters, G. Cotugno, T. H. Johnson, S. R. Clark, and D. Jaksch, "Ab initio derivation of Hubbard models for cold atoms in optical lattices," Phys. Rev. A **87**, 043613 (2013).

[38] T. Johnson, S. Clark, and G. Cotugno, *Wannier states*

for optical lattices (2013), http://ccpforge.cse.rl.ac.uk/gf/project/mlgws/.

[39] M. Grupp, R. Walser, W. P. Schleich, A. Muramatsu, and M. Weitz, "Resonant Feshbach scattering of fermions in one-dimensional optical lattices," J. Phys. B: At. Mol. Opt. Phys. **40**, 2703–2718 (2007).

[40] H. P. Büchler, "Microscopic derivation of Hubbard parameters for cold atomic gases," Phys. Rev. Lett. **104**, 090402 (2010).

[41] M. Olshanii, "Atomic scattering in the presence of an external confinement and a gas of impenetrable bosons," Phys. Rev. Lett. **81**, 938 (1998).

[42] V. Dunjko, V. Lorent, and M. Olshanii, "Bosons in cigar-shaped traps: Thomas-Fermi regime, Tonks-Girardeau regime, and in between," Phys. Rev. Lett. **86**, 5413–5416 (2001).

[43] K. Winkler, G. Thalhammer, F. Lang, R. Grimm, J. H. Denschlag, A. J. Daley, A. Kantian, H. P. Büchler, and P. Zoller, "Repulsively bound atom pairs in an optical lattice," Nature **441**, 853–856 (2006).

[44] For $\eta < 0$, it can be shown that complex conjugate energies produce complex conjugate momenta, thus $k(-\eta) = k^*(\eta)$.

[45] T. Busch, B.-G. Englert, K. Rzażewski, and M. Wilkens, "Two cold atoms in a harmonic trap," Found. Phys. **28**, 549–559 (1998).

[46] L. Xia, L. A. Zundel, J. Carrasquilla, A. Reinhard, J. M. Wilson, M. Rigol, and D. S. Weiss, "Quantum distillation and confinement of vacancies in a doublon sea," Nature Physics **11**, 316320 (2015).